Optics & Laser Technology 164 (2023) 109536

Contents lists available at ScienceDirect

Optics and Laser Technology

journal homepage: www.elsevier.com/locate/optlastec

Full length article

Novel optical method based on nebulization assisted laser induced plasma on inexpensive paper substrates for online determination of halogens and metals in liquid samples

Cristina Méndez-López, Luis Javier Fernández-Menéndez, Cristina González-Gago, Jorge Pisonero, Nerea Bordel *

University of Oviedo, Department of Physics, Federico García Lorca 18, 33007 Oviedo, Asturias, Spain

ARTICLE INFO

Keywords:
LIBS
Liquid sample analysis
Molecular emission
Halogens
Nebulization

ABSTRACT

Halogen determination in liquid matrices with Laser-Induced Breakdown Spectroscopy (LIBS) is still a largely unexplored area of research. Together with the intrinsic problematics of liquid samples in LIBS analysis, halogen atomic emission is hard to observe without experimental modifications (e.g. vacuum chambers for VUV resonant lines or controlled He atmospheres for enhanced IR lines) or without switching to indirect determination via halide molecules emission. For the latter, the presence of an alkali-earth metal element is necessary. Previous works have explored $CaCO_3$ pellets as a substrate provider of Ca, and a nebulization-assisted methodology, with great potential for online implementation, has been successfully tested with synthetic and real F-containing samples. However, manufacturing pellets is a time- and reagent-consuming process not suitable for an online analysis technique and a more convenient substrate is needed. In the present work, different kinds of paper, from regular office paper to oil-painting sheets, are tested to explore its feasibility as a Ca-containing solid target. Different sources of F were also considered including inorganic fluoride and fluorocarbon containing samples. Moreover, both fluorine and chlorine determination via molecular emission are considered, achieving limits of detection (LODs) of 5 ppm and 192 ppm, respectively; a common metal (Zn) is also determined via atomic emission to test its validity for multi-elemental microanalysis, with a LOD of 5 ppm.

1. Introduction

The development of analytical methodologies based on Laser-Induced Breakdown Spectroscopy (LIBS) has been very intense since the beginning of the century due to the numerous advances in instrumentation and data analysis procedures [1]. Although the physical processes involved are complex and still a matter of study themselves, the operating principle of LIBS is fairly simple; a pulsed laser with a short pulse duration (most commonly nanoseconds, but also fs [2] and ps [3]) is focused on a sample in order to achieve a high-enough irradiance, inducing a transient plasma (laser-induced plasma, LIP). The electromagnetic radiation from the plasma includes continuum, ionic, atomic and molecular emission, whose relative importance in the spectra depends on the elapsed time since the laser shot, and which allows for both a determination of the sample composition and a fundamental characterization of the plasma itself. Advantages of LIBS include its versatility, allowing for analysis of solids (metals [4], organic materials [5], powders [6], etc.), liquids (aqueous [7,8], petroleum [9] among others), gases (such as combustion flow fields [10]) and aerosols [11] with little to no sample preparation; the capability for multi-elemental detection, depending on the detection system utilized; its easy implementation as an onsite analysis [12] or online monitoring technique [13] and its potential of scaling for microanalysis purposes in fields such as cultural heritage [14,15] or even medical studies [16,17]. Generally speaking, LIBS offers the possibility of "easily" tailoring experimental setups for the most varied applications, ranging from simple bench commercial instruments to complex arrangements of two [18,19,20] or even three [21] lasers, setups for underwater analysis [22,23], hyphenated systems such as LIBS-Raman for remote analysis [24], etc.

However, LIBS is not without its challenges. Firstly, analysis of liquid samples is subjected to more difficulties than their solid counterparts [25]. Albeit direct analysis on static liquids has long proven to be feasible [26], the increasing demand for robust, high-performance methodologies requires the development of somewhat intricate

* Corresponding author.
E-mail address: bordel@uniovi.es (N. Bordel).

https://doi.org/10.1016/j.optlastec.2023.109536
Received 17 November 2022; Received in revised form 29 March 2023; Accepted 25 April 2023
Available online 5 May 2023

approaches. Strategies can be mainly classified as instrumental modifications or sampling methodologies [7,8], although they are often combined. The first group includes, for example, doble-pulse LIBS [27] or micro-wave-enhanced LIBS [28]. The second includes a broad range of procedures: preconcentration by adsorption [29] or electrochemistry [30], modification of bulk liquid creating a jet flow [31] or an aerosol (via nebulization) [32] and even freezing the liquid [33]. As such, either complex instrumentation or complex sample preparation have to be used.

On the other hand, the elements most commonly analyzed in liquid samples are metals such as Pb, Cd or Cr [8] that do not pose a challenge on themselves, as they can be readily detected by most LIBS configurations. Halogen determination, however, is not so straightforward. These elements have very high ionization and excitation thresholds, and their resonant lines lie within the VUV range. Detection of these elements would require a vacuum chamber or switching to less-intense lines in the IR region. In the latter case, inert gas atmospheres can be used to enhance emission intensity [34,35]. An alternative approach is relying on the molecular emission of a diatomic halogenated molecule product of the recombination of the halogen element and an alkali earth metal in the LIP [36,37]. In absence of the auxiliary element needed for the recombination, previous studies on solid samples have shown that it is possible to add it externally [38,39].

The interest on halogen determination in liquid samples is focused mainly on fluorine, typically added to drinking water to prevent caries, but a health concern if present in high concentrations [40]. The causes of increased concentration can be natural, such as erosion of minerals with a significant amount of fluorine in their composition (e.g. fluorite) or due to human activity, like the use of fertilizers and general industrial activity whose byproducts end up contaminating groundwater [41]. Another example of the latter is the use of fluorocarbon-based fire-extinguishing aqueous film forming foams which, due to the harmful effects of fluorine bioaccumulation, are gradually being substituted by alternative formulations [42]. In this sense, ns-LIBS could potentially be utilized as a quick screening technique to monitor total fluorine and to identify samples with fluorine contamination, without carrying out thorough sample preparation protocols, so that they can be further analyzed in search for specific compounds such as PFASs (per- and polyfluoroalkyl substances) [43]. Other halogens, such as chlorine and bromine, can also be present in drinking water: the former is a commonly present as a salt (NaCl) and is used as a disinfectant, whereas the latter is commonly used for the development of flame retardants, as well as a disinfectant [44]. As with fluorine, health hazards are of particular concern when they are found as organic compounds.

At the moment, research works applying LIBS for the determination of halogens in liquid samples are scarce. Rusak et al. (2015) demonstrated the determination of fluorine via atomic F I emission by using a Surface-Enhanced Raman Spectroscopy (SERS) substrate [45]. These substrates have nanoparticles on their surface, on which the liquid was deposited and ablation performed. Therefore, this could be classified as a NE (Nanoparticle-Enhanced)-LIBS approach. More recently, Tang et al. (2021) utilized a $CaCO_3$ target for determination of F and Cl in liquid samples by depositing 100 μL of the liquid solution with a pipette directly on the solid matrix and heating it afterwards, achieving limits of detection (LODs) of 0.38 ppm and 1.03 ppm for F and Cl, respectively [46].

Our research group implemented a nebulization-assisted LIBS methodology for solid [38] and, recently, liquid [47] F-containing samples analysis. In the first case, a Ca-containing solution was nebulized on the halogenated solid sample providing a LOD of 50 ppm whereas in the second case, a halogenated liquid solution was nebulized on a Ca-based solid target ($CaCO_3$) resulting in a LOD of 10 ppm, a sample consumption of 0.67 μL per repetition and a great potential for online implementation. In this methodology, sample preparation was extremely simple (aqueous dilutions) but solid targets required the mixing of calcium carbonate and amide wax (a binder) followed by hydraulic pressing in order to obtain pellets. This process is not very expensive, but it requires to use an excess of reagents for the pellet to have a suitable thickness that ensures reasonable sturdiness. The time required to make each pellet was also not negligible, nor the need to have steady access to a hydraulic press. Moreover, each pellet could be utilized to perform a maximum of 8 measurements (10 repetitions each) taking advantage of both sides of the pellet and constraining raster lines at a 1 mm distance of each other. This implied that lines were somewhat affected by the nebulization that was performed on the previous line. The contamination of the working space with $CaCO_3$ powder released from the pellets could also be a problem if cleanliness is not carefully maintained. In short, calcium carbonate pellets are useful but not particularly practical in terms of developing a methodology that could be used outside of a research laboratory.

The present work evaluates the use of a low-cost, accessible alternative to calcium carbonate: paper, an everyday material made of a network of bonded fibers, typically manufactured from wood but also from other non-wood alternatives [48]. The availability of paper sheets together with its easy manipulation and versatility make it a very attractive substrate, since they typically contain Ca in the form of calcium carbonate or sulfate, as they are commonly used as filler materials [49]. The only condition that must be sufficed is the presence of calcium in excess as to prevent effects on the quantification of diatomic Ca-halogen molecular signals due to the Ca mass-content of the substrate. Previous research on fluorine determination via nebulization-assisted LIBS in solids established that CaF calibrations required, as a minimum, a 20:1 Ca/F molar ratio [38]. Although the type and quantity (% mass) of filler vary among types and brands of paper, printing papers have quantities of filler in the range of 5–30% [49]. This is well above the halogen concentrations investigated in the present work and hence suitable for this application.

In this research work, further improvements on the fluorine determination methodology are carried out. Moreover, a proof of concept is carried out to illustrate the feasibility of an implementation of the methodology for total fluorine determination in organofluoride-containing samples. Furthermore, the generalization of the methodology for its implementation in the analysis of other elements, such as another halogen (chlorine) and a common metallic element (zinc) is quantitatively studied and critically evaluated.

2. Experimental

2.1. Experimental nebulization-assisted LIBS setup

A full description of the experimental set-up can be found in a previous work [47]. The main elements of this set-up, shown in Fig. 1, are a Nd:YAG laser working at its fundamental wavelength (1064 nm, 3–6 ns, 5 Hz, 100 mJ) and focused with a 35 mm working distance objective. Spot size was estimated to be 400 μm. Light from the laser-induced plasma was collected with two plane convex lenses (50.8 mm diameter, 150 and 300 mm focal lengths) and focused directly onto a 100 μm wide entrance slit of a Czerny-Turner spectrometer (500 mm focal length). Diffraction was performed with a 1200 grooves/mm diffraction grating. Attached to the spectrometer was an ICCD (1024x1024 matrix, pixel size 19 μm). The nebulization set-up consisted of a microflow concentric nebulizer set at ~10 mm over the target surface and with an angle of 50° with respect to the surface, a syringe pump providing a flow rate of 4 μL/min and a mass-flow controller delivering an Ar gas flow of 1 L/min.

2.2. Paper substrates

The role of the solid substrates is fundamental for the determination of the halogen species, as it not only acts as a solid target on which the liquid is deposited and the laser focused, but it also provides the necessary calcium for Ca-X recombination (X being F or Cl). However, a

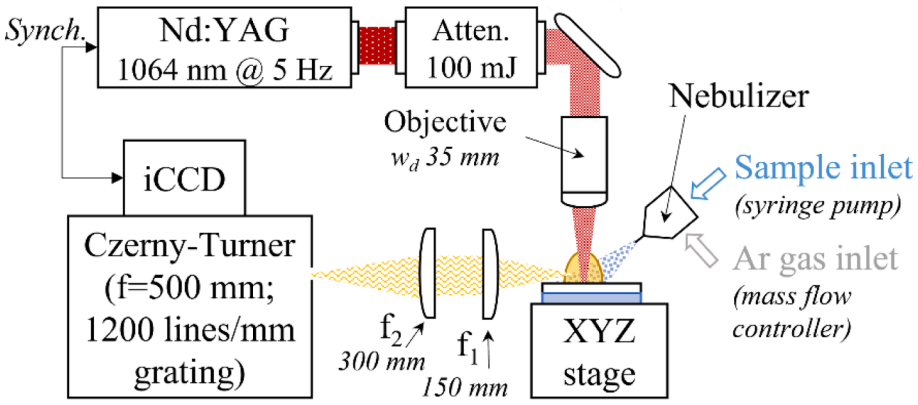

Fig. 1. Schematic diagram showing the main components of the experimental setup.

key aspect of the methodology is to minimize any cost associated to the solid substrate and, following that premise, three ordinary, accessible types of paper were considered: a sheet of regular office paper (80 g/m^2, elemental chlorine free whitened; thickness of 0.12 ± 0.02 mm), a sheet of a common school drawing sketchbook (140 g/m^2; 0.18 ± 0.02 mm) and a sheet of a professional oil-painting paper (290 g/m^2, textured; 0.38 ± 0.02 mm thick).

Substrate preparation was simple and consisted of cutting paper into rectangles of the size of a microscope slide (26 × 76 mm). The rectangles were then fixed onto a slide with double-sided tape. An A4 sheet (210 × 297 mm) was enough to prepare 30 substrates of these dimensions, each of which can contain up to 60 raster lines of 10 mm.

2.3. Nebulization methodology

Measurements were performed by doing two nebulization pre-passes on the target surface in order to deposit the analyte solution before doing a 10 mm long raster of 25 shots at 5 Hz. The solid substrate was displaced at a 2 mm/s speed as optimized in a previous work [47] in terms of signal and stability. This value of speed ensures there is no overlap between spots although each spot may be partially generated in a region affected by the redeposition of the previous laser shot. This last fact does not seem to affect the reproducibility of the measurements probably because the halogen is continuously deposited on the surface of the substrate (as previously mentioned, the nebulizer is working steadily through the measurement and only stopped to refill the syringe with a different solution). The methodology optimized in the previous work was conditioned by the closeness of the raster lines, which was in turn limited by the size of the pellets. The more spacious (and easily replaceable) substrates utilized in the present work allowed a further separation between raster lines of 2 mm, hence avoiding or, at least, minimizing any effect of the nebulization that was directed on the previous lines.

2.4. Nebulization samples

In order to test the procedure with two species of halogens, two sets of aqueous samples were utilized in this work, dissolving suitable salts into Milli-Q water: sodium fluoride for the determination of fluorine, and zinc chloride for the determination of chlorine, in both cases via molecular emission from the species resulting from the recombination with calcium from the substrate (CaF, CaCl). Additionally, the latter set was also utilized for zinc determination as an illustration of the feasibility of performing a multi-elemental characterization of the halogen-containing samples.

The first set of calibration samples corresponds to that described in a previous work [47]. Sodium fluoride (purity 99%, Alfa Aesar) was dissolved on Milli-Q water to obtain a high-concentration solution, which was afterwards further diluted to obtain the concentrations shown in Table 1. Milli-Q water was used as blank throughout the experiment, as it has been shown that nebulization produces significant changes on the physical parameters of the plasma with respect to a non-nebulized case [50].

A sample of an organofluorine-based foam with a theoretical concentration of 1% of fluorine was utilized to verify the capability of ns-LIBS for total fluorine determination of a complex sample containing strong C-F bonds. The sample was diluted taking the calibration range as reference, obtaining two diluted samples of 157 and 372 ppm.

The second set of calibration samples was obtained by dissolving 1.5 g of $ZnCl_2$ (Sigma Aldrich) in 15 g of Milli-Q water together with 0.46 g of 1 M HCl to ensure solubility. Further water dilutions were made to obtain the concentrations shown in Table 2. Naturally, the listed chlorine concentrations take into account the chlorine from the salt as well as the acid. As previously stated, these solutions were also used to test the performance of the methodology for metal detection (Zn) through atomic emission signal. Due to the higher sensitivity of detection for the metal element, two additional solutions were prepared containing 108 ppm and 16 ppm of Zn (Zn_1 and Zn_2), respectively.

3. Results and discussion

3.1. Selection of the paper substrate

The first step to evaluate their suitability was subjecting the different papers to both nebulization of ultrapure water (blank) and laser ablation. It is worth remarking that care should be taken when defining the target displacement speed with respect to the repetition rate of the laser, avoiding spot overlapping. Particularly, in a previous work [47], a detailed study regarding these parameters was carried out ensuring that, in all cases considered, the distance between spots was roughly the spot diameter. From this study, it was concluded that a displacement speed of 2 mm/s, with its corresponding frequency rate of 5 Hz, was the most adequate to both avoid damage due to excessive humidification of the target while still allowing for a significant deposition of the analyte.

Under said experimental conditions, it was seen that no apparent damage, aside from the obvious ablated lines, was present. The laser

Table 1
Calibration samples used for fluorine determination.

Sample	[F] (ppm)	Sample	[F] (ppm)
B	0	F_6	252
F_1	12	F_7	342
F_2	25	F_8	481
F_3	54	F_9	613
F_4	112	F_10	860
F_5	161	F_11	1429

Table 2
Calibration samples used for chlorine and zinc determination.

Sample	[Cl] (ppm)	[Zn] (ppm)	Sample	[Cl] (ppm)	[Zn] (ppm)
B	0	0	Cl_6	2438	2118
Cl_1	255	221	Cl_7	3625	3149
Cl_2	449	390	Cl_8	4590	3988
Cl_3	734	638	Cl_9	6261	5440
Cl_4	1153	1001	Cl_10	8410	7307
Cl_5	1761	1530			

configuration of energy and distance between shots was not enough to completely get through the paper even for the thinnest of the ones considered (office paper). On the other hand, the nebulization was not seen to wet the sheets to the point of damaging them. A general image of a drawing paper substrate after being subjected to ablation and nebulization, as well as a more detailed inset, can be seen in Fig. 2.a. The raster lines produced by the laser ablation are clearly distinguished due to the high fluence utilized in this work but for neither of the three paper substrates a complete ablation of the sheet is produced. The decrease of thickness in the ablated area, however, can be qualitatively pointed out by visual inspection against a light source. Avoiding the ablation of the underlying double-sided tape throughout the whole raster line is of the uttermost importance, as the change in chemical composition would alter the spectra to some extent. Fig. 2.b shows a backlit image of the drawing paper with the craters resulting from six sequences of bursts ranging from 1 to 25 shots (4 repetitions), performed under simultaneous nebulization of ultrapure water. It is seen that transparency becomes perceivable at 5 shots in 3 out of the 4 repetitions and very notable for 10 shots onwards. This shows that there is no significant risk of ablating the material underneath the paper sheet even if a small overlapping of the raster spots took place.

The second step was evaluating the qualitative composition of each sheet. For this purpose, a full spectrum from 250 to 700 nm was obtained for each of the sheets in the 30–35 μs time window, taken as reference as it was the optimized value obtained in previous studies with a $CaCO_3$ substrate [47]. In order to maintain the working conditions of the experiment, these measurements were also done while nebulizing ultrapure water (our blank). The spectra corresponding to each type of paper were seen to be mostly analogous, but the key differences can be seen in the 510–630 nm region that is shown in Fig. 3. It is immediately evident that the oil painting paper has a very significant amount of fluorine, as evidenced by the prominent CaF emission bands. The office and drawing papers are much more similar, with the main difference being the content of Mg (higher for the drawing paper, although present in all of them) and, more importantly, the presence of Cl in the office paper (revealed by a discreet signal from the CaCl orange system at 593 nm). Given that the objective of this work is mainly the determination of F and Cl, it was made clear that the most suitable substrate was the drawing paper as the intended blank measurements were, indeed, blanks in both cases.

It is important to note that this choice does not completely discard "office papers" as a suitable blank for some applications other than chlorine determination. According to the manufacturer information, this particular office paper was whitened by an elemental chlorine free (ECF) technique. Alternatively, a totally chlorine free (TCF) office paper would not present this issue. In any case, a complete spectral characterization of the paper should be carried out before applying this methodology. Nevertheless, an advantage of the drawing paper is that its grammage and thickness facilitate the substrate preparation as compared to a thinner regular office paper, minimizing irregularities on the surface when fixing it to the lab slide.

3.2. Optimization of the acquisition conditions

Once the substrate was chosen, the optimization of the delay time for CaF and CaCl acquisition was explored, respectively. Firstly, because the temporal window previously considered for CaF cannot be assumed to still be the optimum, as the matrix has been changed, but also because the virtually unlimited availability of this type of target allowed us to perform here a much more detailed study of the emission evolution. In particular, two spectral windows were considered: one for fluorine determination (516.4 – 549.6 nm) via emission from the sequence $\Delta\nu = 0$ of system $B^2\Sigma - X^2\Sigma$ of CaF and another one for chlorine determination (576.5–609.5 nm) via emission from the sequence $\Delta\nu = 0$ of system $B^2\Sigma - X^2\Sigma$ of CaCl. The calibration samples F_8 and Cl_ 7 containing 481 ppm of fluorine and 3625 ppm of chlorine, respectively, were chosen to perform this optimization. In addition, ultrapure water was nebulized as blank for measurements in both wavelength exposures. The 25 time windows that were considered for this optimization are shown in Table 3.

Data treatment to obtain the integrated areas was similar to the procedures previously illustrated in [47,51]. A detailed step-by-step description is provided as Supplementary material (Section 1). The method consisted of four stages: (1) the raw spectra (Fig. 4.a-b) were normalized to a spectral region corresponding to calcium oxide emission (present in both CaF and CaCl spectral windows). Afterwards, (2) an average of the normalized blank was obtained and subtracted from each individual spectrum, removing the interfering signal. Then, (3) the atomic interferences were removed via suitable polynomic fits. (4) The baseline is adjusted, and emission is integrated in the corresponding spectral range (Fig. 4.c-d, see vertical lines).

The spectra acquired at delays shorter than 20 μs were discarded due to the high atomic emission. The integrated areas from the remaining spectra were combined to form five potential acquisition windows both for CaF and CaCl detection: (20–24 μs), (22–30 μs), (28–40 μs), (35–60 μs) and (45–75 μs). The subsequent analysis was performed by evaluating various aspects: firstly, that the maximum absolute signal in the raw spectral windows (both blanks and analytes) did not surpass the linear range of the ICCD. Secondly, that the net analyte signals from the raw spectra were as high as possible to improve signal-to-noise ratios.

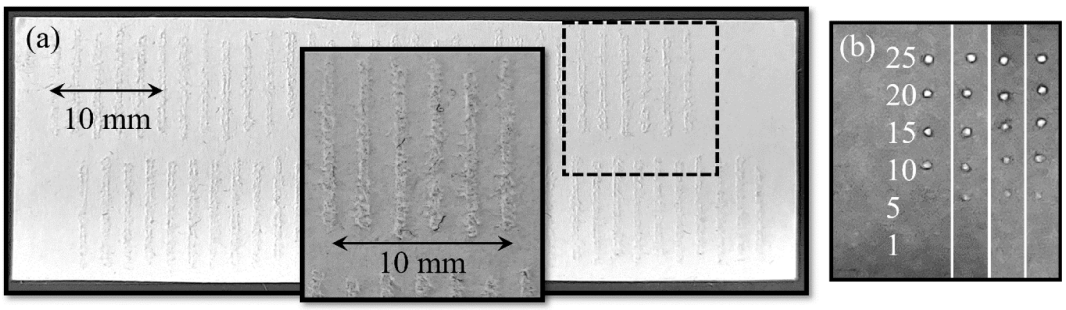

Fig. 2. (a) A drawing paper sample utilized for nebulization experiments, showing a detailed inset for 6 raster lines. (b) Detail of craters for six different burst numbers (4 repetitions). Brightness and contrast of the images have been modified for visualization purposes.

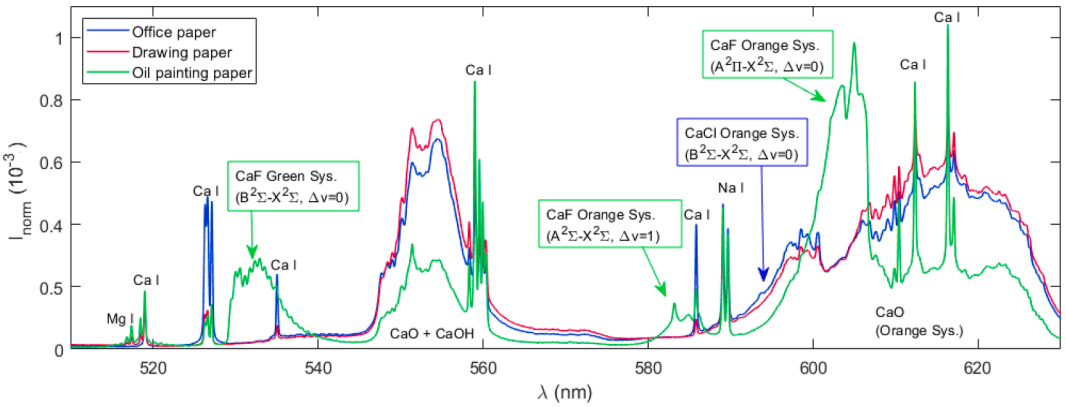

Fig. 3. Spectra of the three paper sheets evaluated as substrates.

Table 3
Time windows utilized for the temporal evolution study. Note that all expositions from delay 20 μs onwards are contiguous (i.e. time windows start where the previous ends).

Delay range (μs)	Delay step (μs)	Gate (μs)
1–5	1	0.5
6–18	2	1
20–28	2	2
30–60	5	5
65	–	10

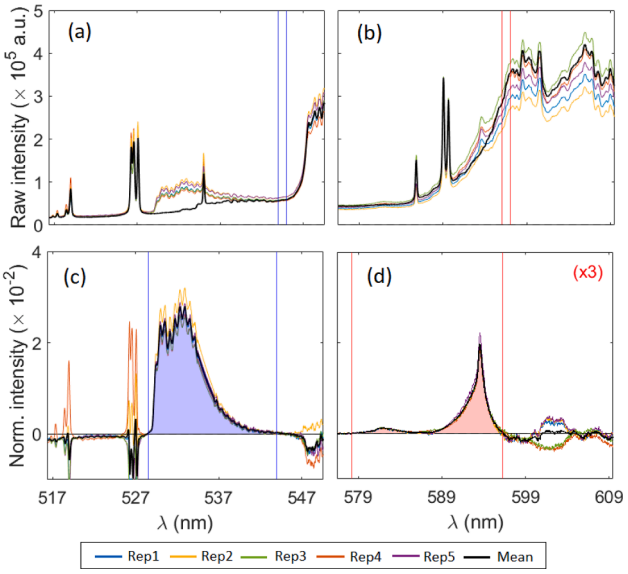

Fig. 4. Comparison of the raw spectra obtained for (a) CaF and (b) CaCl, indicating the normalization region with vertical lines, and the resulting spectra after full data treatment procedure for (c) CaF and (d) CaCl, indicating the integration region.

Thirdly, that RSDs were moderate both for the raw signals and, more importantly, for the normalized signals. The full analysis is included in the Supplementary material (Section 2).

The first criteria resulted in the elimination of (22–30 μs) window for CaF and of (35–60 μs) window for CaCl. The second and third criteria allowed the selection of the optimum windows shown in Table 4 together with the relevant figures of merit.

Table 4
Optimum acquisition windows for CaF and CaCl detection.

Species	Optimum window	Net intensity (10^7 a.u.)	Norm. intensity RSD
CaF	35–60 μs	2.4 ± 0.2	4%
CaCl	22–30 μs	0.75 ± 0.04	5%

3.3. Calibration curves

3.3.1. Fluorine determination

The nebulization and LIBS analysis of the calibration samples shown on Table 1 was carried out by performing 10 repetitions per sample and replacing the paper target after every five to six samples. Measurements were done strictly from low to high concentrations. The data treatment procedure was mostly the same as shown in Section 3.2. Fig. 5 shows the average spectra for each sample at every step of the data processing: normalization (Fig. 5.a.), blank subtraction (Fig. 5.b) and final spectra after atomic emission removal and baseline correction (Fig. 5.c.). It is seen that the normalization to the CaO/CaOH signal in order to subtract the blank signal worked remarkably well for this spectral window. It's worth noting that the blank signal is, firstly, used to produce an average normalized blank spectrum and then processed as the rest of the sample spectra (i.e. the average normalized blank is subtracted from each of the normalized blank repetitions).

The final step, integrating the molecular emission, was changed from the temporal studies procedure. Instead of integrating between two fixed limits a variable range was implemented, similar to what was shown in a previous work regarding Cl determination [51]. The maximum of the molecular emission bands of interest (i.e. CaF and CaCl) was determined in between the fixed integration limits and then, the wavelengths at which intensity first lowered to 2% of its maximum were set as new integration limits. For the next lower concentration, the same procedure was applied but setting the extra condition that integration limits could either become narrower or be maintained. Finally, the integration limits for the blank were the same as for the lowest concentration sample. Fig. 5.c. shows the broadest and narrowest integration ranges, which differ a total of 4 nm. Of course, the left limit suffers the least variation due to the steep slope of the band head.

The resulting calibration curve is shown in Fig. 6. The linear range extends up to approximately 900 ppm, lower than the highest [F] calibration sample (F_11), which was excluded for the linear fit computation. This result is in agreement with that obtained for the calibration on a $CaCO_3$ pellet [47]. Moreover, both the new limit of detection (5 ppm), calculated according to the 3σ criterium (three times the uncertainty of the blank signal divided by the slope), and the linearity of the calibration were improved in the present work, suggesting that paper is a better target than pellets. Indeed, irregularities observed on the rasters carried

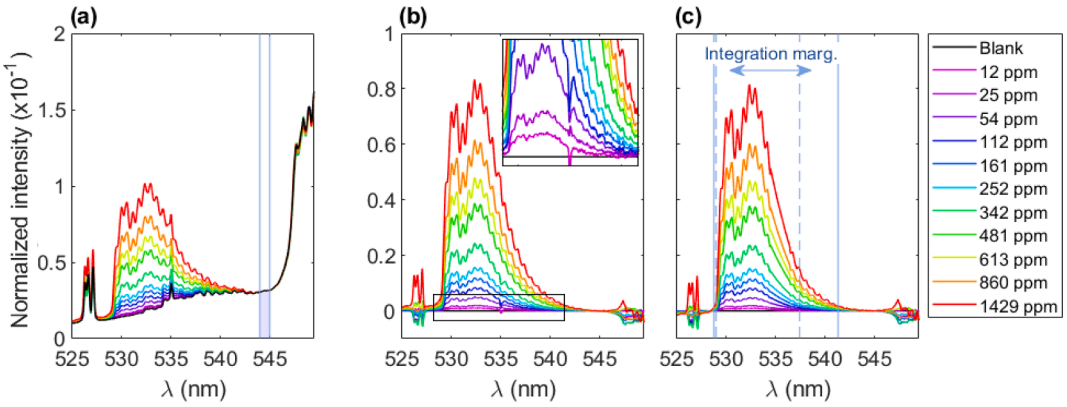

Fig. 5. Steps of the data treatment procedure shown for the whole F calibration set: (a) average raw spectra with normalization region indicated with vertical lines, (b) normalized spectra after blank subtraction, with lowest concentrations shown as inset, and (c) normalized spectra after interfering line removal and baseline correction; widest and narrowest integration regions are shown with continuous and dotted lines, respectively.

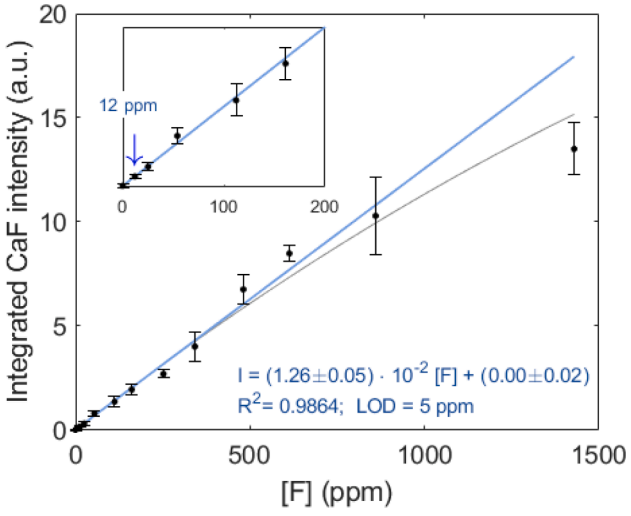

Fig. 6. Calibration curve for fluorine determination.

out on pellets are absent on the paper targets.

In order to further test the validity of these results and considering the limited number size of the calibration samples set, a Leave-One-Out Cross-Validation (LOOCV) procedure was carried out. In this method, a sample is taken out of from the calibration set and it's afterwards used to test it. For this purpose, 10 calibration curves were built. For each of them, the concentration of one of the samples (F_1,…,F_10) was determined with the calibration curve obtained using the remaining 9 samples and blank. Results from this analysis are given in Table 5. The Root Mean Square Relative Error (RMSRE) was chosen as parameter of evaluation for LOOCV, defined in Equation (1) as follows:

Table 5
Results of the LOOCV analysis of the fluorine determination dataset.

	Full set calibration curve	LOOCV		
		RMSRE (%)	11	
		$\overline{P}$	$STD(\overline{P})$	$\delta\overline{P}$
Slope (a.u./ ppm)	(0.0126 ± 0.0005)	0.0125	0.0004	0.0002
Intercept (a.u.)	(0.00 ± 0.02)	−0.002	0.003	0.006
R^2	0.9864	0.987	0.003	–
LOD (ppm)	5	5.18	0.16	–
Strict LOD (ppm)	7	6.9	0.6	–

$$RMSRE(\%) = \sqrt{\frac{1}{N}\sum\left(\frac{x_{est} - x_0}{x_0}\right)^2}\cdot 100\% \quad (1)$$

where N is the number of iterations, x_{est} is the concentration calculated from the calibration curve and x_0 is the nominal value of the concentration. Two quantities are shown in order to provide an estimation of the uncertainty of the average values obtained for the slope and the intercept. Firstly, the standard deviation (STD) of the average of a parameter P is calculated according to Equation (2), in which p_i denotes each value of the parameter; this value provides information about the different results that are obtained from the calibrations for each parameter.

$$STD(\overline{P}) = \sqrt{\frac{1}{N-1}\sum(p_i - \overline{P})^2} \quad (2)$$

Secondly, as the previous parameter doesn't take into account the uncertainty provided by the Least-Squares method for each of those results (e.g. $p_i \pm \delta p_i$), an uncertainty is propagated as shown in Equation (3).

$$\delta\overline{P} = \sqrt{\sum\left(\frac{\partial\overline{P}}{\partial p_i}\right)^2 \delta p_i^2} = \frac{1}{N}\sqrt{\sum \delta p_i^2} \quad (3)$$

Additionally, in order to test the influence of the uncertainties in the calibration curve parameters, a more strict definition of LOD [52] was computed, in which the errors of the slope and intercept are not neglected, as shown in Equation (4).

$$LOD_{strict} = \frac{3\sqrt{\sigma_B^2 + \delta n^2 + \left(\frac{n}{m}\right)^2 \delta m^2}}{m} \quad (4)$$

where σ_B is the standard deviation of the blank, m is the slope of the calibration curve, n is the intercept, and δm, δn are the corresponding errors. Of course, when these errors are very small, the expression reduces to the usual 3·sigma.

The LOOCV procedure provided a RMSRE of 11%. This value is reasonably moderate to be considered acceptable. It is worth noting that the slope is well-maintained, with little deviation from the mean (3%) and determined with high precision in the Least Squares fitting procedure (<2% propagated uncertainty). For the intercept there are significant fluctuations around the mean, albeit this variation is within the uncertainty range with which this parameter is determined. The coefficient of determination (R^2) is very similar in all cases, staying close to $R^2 = 0.99$. Finally, limits of detection are also maintained throughout the study at 5 ppm. It is remarkable that, considering the sample consumption of 1 μL/line, this corresponds to 5 ng of F (0.26 nmol). The stricter LOD expression provides a slightly higher value of 7 ppm, with

the main source of increment being an intercept error comparable to the blank standard deviation.

3.3.2. Proof of concept: Feasibility of total F determination for organofluorine-containing samples

In order to evaluate the capability of this methodology for analysis of complex samples containing fluorine-carbon bonds, a direct, qualitative comparison of the normalized emission obtained from the nebulization of the blank, a NaF reference sample (F_5) and the two diluted foam samples is shown in Fig. 7. Firstly, a similar CaF emission intensity can be observed for the reference and foam samples of equivalent fluorine concentration. In fact, slightly higher intensity is observed for the foam sample. This suggests that the native bonds of fluorine are not playing a significant role for determination of total fluorine, in this range of concentrations, as they are indeed broken in the nanosecond-laser ablation process. Moreover, the inset graph shows that a proportional increase in emission is obtained for the foam samples, strengthening the feasibility of implementing this methodology for the analysis of complex organofluorine samples without need of further sample preparation.

3.3.3. Chlorine determination

Analogously to the previous case, 10 repetitions were carried out for each of the calibration samples shown in Table 2. The paper targets were replaced every 5–6 samples, and the order of measurements was again from low to high concentrations. The main steps of data treatment are shown in Fig. 8 for the different concentrations, particularly the normalized spectra (Fig. 8.a.), the spectra after background subtraction (Fig. 8.b.) and the spectra after removing the emission lines and correcting the baseline (Fig. 8.c.). As previously indicated, a variable range of integration was implemented to optimize the calibration procedure. The same criteria of limiting the range to the value of 2% of maximum intensity and forcing the integration window to either be narrower or the same as the one obtained for the next-higher concentration was maintained. Similarly to what was obtained for CaF, the limit corresponding to the steeper variation of intensity in sequence $\Delta v = 0$ remains practically unchanged unlike the limit corresponding to sequence $\Delta v = 1$.

The calibration curve built for the chlorine samples set is shown in Fig. 9.

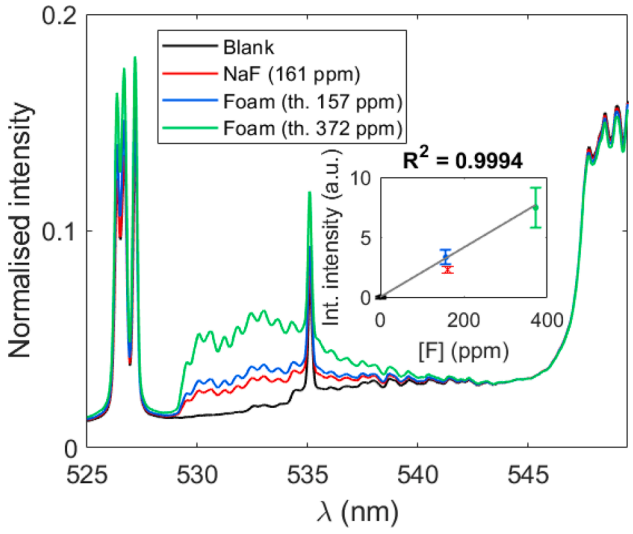

Fig. 7. Comparison of the normalized emission nebulizing ultrapure water (blank), diluted foam samples (157 and 372 ppm) and sodium fluoride (161 ppm). Inset shows a linear fit for the blank and foam samples. The red data point corresponds to the equivalent integrated value for the NaF sample. (For interpretation of the references to colour in this figure legend, the reader is referred to the web version of this article.)

The linearity of the calibration is maintained throughout the entire concentration range, therefore extending up to almost 9000 ppm. This is an order of magnitude more than the linear range obtained for fluorine (Fig. 6) but the limits of detection are also much higher, at 192 ppm.

An analogous LOOCV analysis to the one shown for fluorine was carried out to further examine the proposed calibration, displaying the results in Table 6.

For this set of calibrations, a more reduced RMSRE of 6% is obtained (almost half of that of fluorine). Both the variation of the determined slopes and the uncertainty of the parameter are very small, well below 1%. The intercept is more prone to change, observing variations in the range of 10%, which might be again explained due to the lower precision with which this parameter is determined in the linear fitting procedure. The linearity of all the calibration curves is very high, with $R^2 > 0.99$. The limits of detection obtained in each case show little variation and are maintained at 192 ppm. Considering the sample consumption of 1 μL/line, this corresponds to 192 ng of Cl (5.4 nmol). In this case, the increment from the stricter definition of LOD is more reduced, since the error of the intercept is smaller than the standard deviation of the blank. As with fluorine, the error of the slope was negligible and did not contribute to increase the LOD.

3.3.4. Extension of the methodology to other elements

Lastly, the Zn content of the chlorine solutions was used to build calibration curves for a common metal element. Fig. 10 shows two average spectra (from 461.3 to 494.7 nm) in the 4–5 μs time window, one for a concentration of 7307 ppm and the other corresponding to the blank spectrum. Most of the spectrum was utilized for normalization, excluding two regions (466.5–473.0 and 480.2–481.8 nm) where the emission of Zn I is located. This is indicated in Fig. 10 by means of colored areas. The main emission lines are labeled and correspond to Zn I (468.01, 472.22 and 481.05 nm) and alkali-earth metals: Ca I (468.53 and 487.81 nm), Mg I (470.30 nm), and Ba II (493.40 nm). The first line of Zn I was discarded due to the interference with Ca I, and the sum of the integrated intensity of the remaining two Zn I lines was used as analytical signal.

The data treatment procedure (see Fig. 11) was analogous to that of the molecular signals. All spectra (Fig. 11.a) were normalized (Fig. 11.b) and an average value of the normalized blank was obtained and subtracted from each spectrum. Then, a linear baseline was fit and removed to correct the region of interest (Fig. 11.c). Finally, a variable range integration was performed with the same criteria than the molecular one.

The resulting calibration plot (Fig. 12) revealed a non-linear behaviour in the considered concentration range. This behaviour is well-modelled by a power function with exponent 0.72 ± 0.04 (shown in purple). The point corresponding to 5440 ppm was excluded from the linear fit as it was identified as an outlier. For low concentrations up to 638 ppm, which are highlighted as an inset plot, a linear calibration curve with a sharp slope (shown in green) could be approximated. The limits of detection were calculated to be 5 ppm, which is, for 1 μL/line, a mass of 5 ng, or an amount of 0.08 nmol. It's worth noting that this LOD was maintained when implementing the stricter LOD definition of Equation (4).

The mechanism behind the deviation from linearity that is observed for Zn concentrations greater than 600 ppm is not clear. Self-absorption does not seem to be responsible for this effect since a negligible variation of the FWHM of line Zn I 472.22 nm with respect to Zn concentration was observed. Further studies out of the scope of this manuscript would therefore be required to elucidate the origin of this non-linear behaviour, which could be related to incomplete atomization of the ablated matter or other matrix effects [53].

The feasibility of using paper as a substrate also for metallic species that don't need to recombine has been demonstrated in this work.

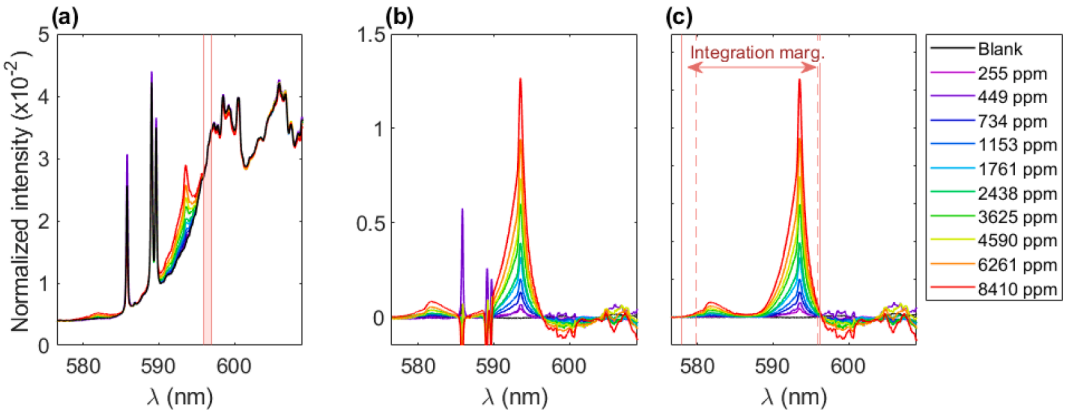

Fig. 8. Steps of the data treatment procedure shown for the whole Cl calibration set: (a) average normalized spectra, (b) blank-removed spectra (c)spectra after atomic-lines removal and baseline correction. Narrowest and broader integration ranges are indicated by means of dotted and continuous lines, respectively.

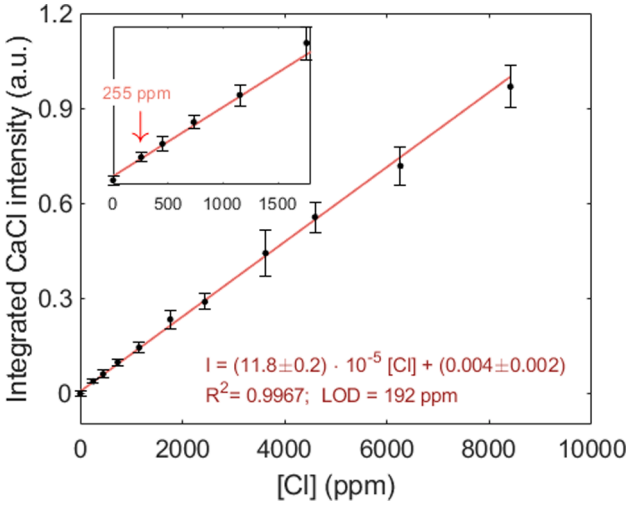

Fig. 9. Calibration curve for chlorine determination.

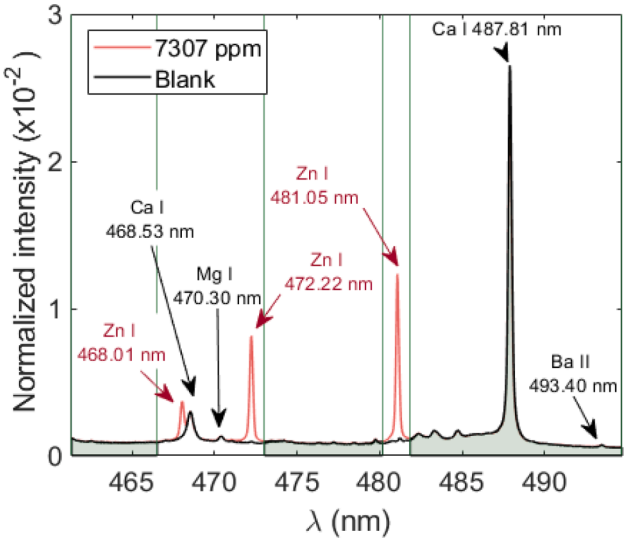

Fig. 10. Spectral region utilized to detect Zn. Green-colored area corresponds to the normalization region. (For interpretation of the references to colour in this figure legend, the reader is referred to the web version of this article.)

Table 6
Results of the LOOCV analysis of the chlorine determination dataset.

	Full set calibration curve	LOOCV		
		RMSRE (%)	6	
		$\overline{P}$	$STD(\overline{P})$	$\delta\overline{P}$
Slope (× 10^{-5} a.u./ ppm)	(11.8 ± 0.2)	11.85	0.07	0.08
Intercept (a.u.)	(0.004 ± 0.002)	0.0039	0.0004	0.0008
R^2	0.9967	0.9966	0.0004	–
LOD (ppm)	192	192.0	1.2	–
Strict LOD (ppm)	202	202	2	–

4. Conclusions

In the present work, regular paper was studied as a cheap, versatile, and accessible Ca-containing solid substrate for halogen determination in a nebulization-assisted LIBS methodology. Particularly, office, drawing and oil-painting papers were considered, deeming that drawing paper was the most appropriate choice due to its lack of fluorine and chlorine (within the methodology's limits of detection) and its thickness, which facilitated that no irregularities were produced during substrate preparation. Said process is extremely simple, merely consisting in attaching paper onto a lab slide. This solid substrate significantly reduces time, reagents and instrumentation requirements as compared to the previously proposed substrate ($CaCO_3$ pellets) and strengthens the potential of the methodology for its online implementation.

After a thorough optimization process thanks to the availability of target substrate (paper), three highly linear calibration curves were obtained using two sets of samples with known F, Cl and Zn content. The limits of detection obtained for fluorine were improved (5 ppm) with respect to a previous work (10 ppm) [47], and the applicability to both another halogen (chlorine, LOD of 192 ppm) and a metallic element (zinc, LOD of 5 ppm) were demonstrated. The LOD reported for chlorine is almost 40 times that of fluorine, partly due to the much lower intensity of the CaCl emission bands with respect to the CaF emission. Additionally, another important factor that has to be considered is the high intensity of CaO emission with respect to the CaF/CaCl emissions; this is particularly important for CaCl determination, which is much more strongly interfered by CaO as well as by Na I, making data treatment a very delicate procedure. Minimizing the amount of oxygen present in the plasma would be desirable, but both Ca-containing targets that have been considered have it as a matrix element ($CaCO_3$ in [47] and cellulose, in the present work), not to mention the liquid matrix (H_2O) and the air atmosphere. Further optimizations have to be considered in order to reduce these relative LODs and be able to rely on this methodology for the most demanding applications. However, as a microanalysis

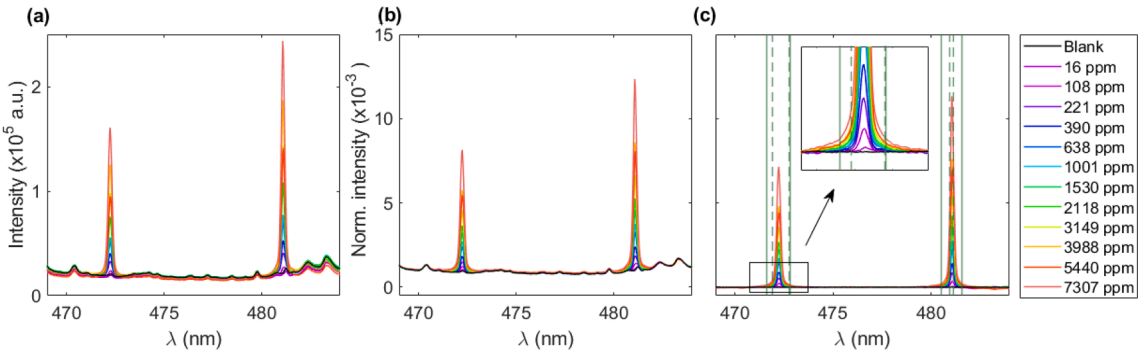

Fig. 11. Region of interest (from 469 to 484 nm) at different stages of data treatment, namely (a) average raw spectra, (b) average Ca-normalized spectra and (c) average blank-subtracted, baseline-corrected spectra. The widest and narrowest integration ranges are shown with continuous and dotted vertical lines, respectively. Inset shows detail of Zn I at 472.22 nm for lowest concentrations.

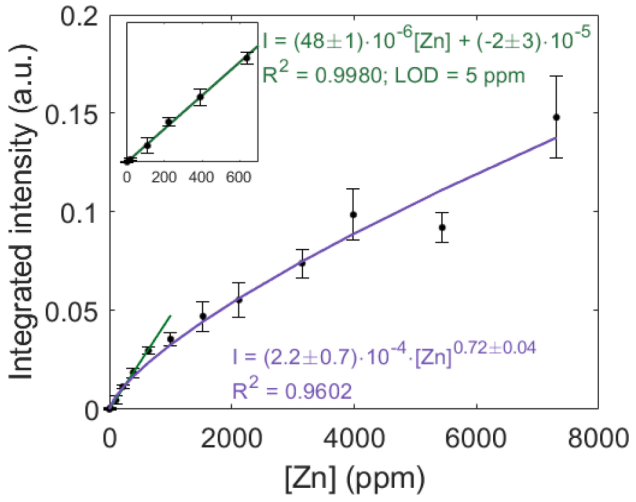

Fig. 12. Calibration curves for Zn content. Inset shows the blank and lowest concentration data point.

methodology requiring only 1 μL of sample per repetition, the absolute limits of detection were as low as 5, 192 and 5 ng for F, Cl and Zn, respectively.

Additionally, a proof of concept was carried out by analyzing two diluted samples of a fluorosurfactant-based foam. This study showed that a comparable CaF signal was obtained from the fluorocarbon sample with respect to the inorganic sodium fluoride, proving that a total fluorine analysis in such complex samples is feasible with ns-LIBS without adding further sample preparation steps. Furthermore, although a more thorough analytical characterization of these samples is still needed, a linear relationship was observed when performing a tentative comparison of the emission from the blank signal and the two diluted foam samples (157 and 372 ppm).

CRediT authorship contribution statement

Cristina Méndez-López: Conceptualization, Methodology, Investigation, Formal analysis, Visualization, Writing – original draft, Writing – review & editing. **Luis Javier Fernández-Menéndez:** Conceptualization, Methodology, Writing – review & editing. **Cristina González-Gago:** Supervision, Writing – review & editing. **Jorge Pisonero:** Conceptualization, Supervision, Writing – review & editing, Funding acquisition. **Nerea Bordel:** Conceptualization, Supervision, Writing – review & editing, Funding acquisition.

Declaration of Competing Interest

The authors declare that they have no known competing financial interests or personal relationships that could have appeared to influence the work reported in this paper.

Data availability

The data that has been used is confidential.

Acknowledgements

This work was supported by the Spanish Government (projects MCI-21-PID2020-113951GB-I00/AEI/10.13039/501100011033 and MINECO BES-2017-080768) as well as by the Principality of Asturias (through predoctoral grant "Severo Ochoa" PA-21-PF-BP20-059 and grant SV-PA-23-AYUD/2022/33582). The assistance provided by the Environmental Testing unit of the University of Oviedo Scientific-Technical Services (SCTs) is also thankfully acknowledged.

Appendix A. Supplementary data

Supplementary data to this article can be found online at https://doi.org/10.1016/j.optlastec.2023.109536.

References

[1] G. Galbács, A critical review of recent progress in analytical laser-induced breakdown spectroscopy, Anal. Bioanal. Chem. 407 (25) (2015) 7537–7562.
[2] T. Labutin, V. Lednev, A. Ilyn, A. Popov, Femtosecond laser-induced breakdown spectroscopy, J. Anal. At. Spectrom. 31 (1) (2016) 90–118.
[3] A. Marín Roldán, V. Dwivedi, M. Pisarčík, et al., LIBS investigation of metals suitable for plasma-facing components: Characteristics and comparison of picosecond and nanosecond regimes, Fusion Eng. Des. 172 (2021), 112898.
[4] X. Li, Y. Guan, Theoretical fundamentals of short pulse laser-metal interaction: A review, Nanotechnol. Precis. Eng. 3 (3) (2020) 105–125.
[5] J. Moros, J. Laserna, Laser-Induced Breakdown Spectroscopy (LIBS) of Organic Compounds: A Review, Appl. Spectrosc. 73 (9) (2019) 963–1011.
[6] S. Pandey, R. Locke, R. Gaume, et al., Effect of powder compact density on the LIBS analysis of Ni impurities in alumina powders, Spectrochim. Acta Part B 148 (2018) 99–104.
[7] X. Yu, Y. Li, X. Gu, J. Bao, H. Yang, L. Sun, Laser-induced breakdown spectroscopy application in environmental monitoring of water quality: a review, Eniron. Monitor. Assess. 186 (2014) 8969–8980.
[8] K. Keerthi, S.D. George, S. Kulkarni, et al., Elemental analysis of liquid samples by laser induced breakdown spectroscopy, Opt. Laser Technol. 147 (2022) 107622.
[9] A. Bol'shakov, S. Pandey, X. Mao, et al., Analysis of liquid petroleum using a laser-induced breakdown spectroscopy instrument, Spectrochim. Acta B 179 (2021), 106094.
[10] D. Zhang, Q. Gao, B. Li, et al., Instantaneous one-dimensional equivalence ratio measurements in methane/air mixtures using femtosecond laser-induced plasma spectroscopy, Opt. Exp. 27 (3) (2019) 2159.
[11] D. Palásti, A. Metzinger, T. Ajtai, et al., Qualitative discrimination of coal aerosols by using the statistical evaluation of laser-induced breakdown spectroscopy data, Spectrochim. Acta Part B 153 (2019) 34–41.

[12] S. Pérez-Diez, L.J. Fernández-Menéndez, M. Veneranda, et al., Chemometrics and elemental mapping by portable LIBS to identify the impact of volcanogenic and non-volcanogenic degradation sources on the mural paintings of Pompeii, Anal. Chim. Acta 1168 (2021), 338565.
[13] H. Kim, J. Lee, E. Srivastava, et al., Front-end signal processing for metal scrap classification using online measurements based on laser-induced breakdown spectroscopy, Spectrochim. Acta Part B 184 (2021), 106282.
[14] V. Spizzichino, R. Fantoni, Laser Induced Breakdown Spectroscopy in archeometry: A review of its application and future perspectives, Spectrochim. Acta Part B 99 (2014) 201–209.
[15] V. Detalle, X. Bai, The assets of laser-induced breakdown spectroscopy (LIBS) for the future of heritage science, Spectrochim. Acta Part B 191 (2022), 106407.
[16] B. Busser, S. Moncayo, J. Coll, et al., Elemental imaging using laser-induced breakdown spectroscopy: A new and promising approach for biological and medical applications, Chem. Rev. 358 (2018) 70–79.
[17] R. Gaudiuso, E. Ewusi-Annan, N. Melikechi, et al., Using LIBS to diagnose melanoma in biomedical fluids deposited on solid substrates: Limits of direct spectral analysis and capability of machine learning, Spectrochim. Acta Part B 146 (2018) 106–114.
[18] C. Gautier, P. Fichet, D. Menut, et al., Applications of the double-pulse laser-induced breakdown spectroscopy (LIBS) in the collinear beam geometry to the elemental analysis of different materials, Spectrochim. Acta Part B 61 (2) (2006) 210–219.
[19] C. Ahamer, J. Pedarnig, Femtosecond double pulse laser-induced breakdown spectroscopy: Investigation of the intensity enhancement, Spectrochim. Acta Part B 148 (2018) 22–30.
[20] H. Sobral, R. Sanginés, Comparison of plasma parameters and line emissions of laser-induced plasmas of an aluminum target using single and orthogonal double nanosecond/picosecond pulses, Spectrochim. Acta Part B 94–95 (2014) 1–6.
[21] D. Prochazka, P. Pořízka, J. Novotný, et al., Triple-pulse LIBS: Laser-induced breakdown spectroscopy signal enhancement by combination of pre-ablation and re-heating laser pulses, J. Anal. At. Spectrom. 35 (2) (2020) 293–300.
[22] S. Guirado, F. Fortes, J. Laserna, Elemental analysis of materials in an underwater archeological shipwreck using a novel remote laser-induced breakdown spectroscopy system, Talanta 137 (2015) 182–188.
[23] J. Guo, Y. Lu, K. Cheng, et al., Development of a compact underwater laser-induced breakdown spectroscopy (LIBS) system and preliminary results in sea trials, Appl. Opt. 56 (29) (2017) 8196–8200.
[24] K. Muhammed Shameem, V. Dhanada, S. George, et al., Assessing the feasibility of a low-throughput gated echelle spectrograph for Laser-induced Breakdown spectroscopy (LIBS)-Raman measurements at standoff distances, Opt. and Laser. 153 (2022), 108264.
[25] V. Lazic, S. Jovićević, Laser induced breakdown spectroscopy inside liquids: Processes and analytical aspects, Spectrochim. Acta Part B 101 (2014) 288–311.
[26] D. Cremers, L. Radziemski, Spectrochemical analysis of liquids using the laser spark, Anal. Chem. 38 (1984) 721–729.
[27] H. Harun, R. Zainal, Laser-induced breakdown spectroscopy measurement for liquids: Experimental configurations and sample preparations, J. Nonlinear Opt. Phys. Mater. 27 (2018) 1850023.
[28] Y. Ikeda, Determining the detection limit of Strontium, Calcium, and Lead in an aqueous jet using microwave-enhanced plasma-ball optical emission spectrometry, Talanta 6 (2022), 100137.
[29] A. Haider, M. Ullah, Z. Khan, et al., Detection of trace amount of arsenic in groundwater by laser-induced breakdown specroscopy and adsorption, Opt. Laser Technol. 56 (2014) 299–303.
[30] F. Zhao, Z. Chen, F. Zhang, et al., Ultra-sensitive detection of heavy metal ions in tap water by laser-induced breakdown spectroscopy with the assistance of electrical-deposition, Anal. Methods 2 (4) (2010) 408–414.
[31] K. Skočovská, J. Novotný, D. Prochazka, et al., Optimization of liquid jet system for laser-induced breakdown spectroscopy analysis, Rev. Sci. Instrum. 87 (2016), 043116.
[32] M. Sui, Y. Fan, L. Jiang, et al., Online ultrasonic nebulizer assisted laser induced breakdown spectroscopy (OUN-LIBS): An online metal elements sensor for marine water analysis, Spectrochim. Acta Part B 180 (2021), 106201.
[33] H. Sobral, R. Sanginés, A. Trujillo-Vázquez, Detection of trace elements in ice and water by laser-induced breakdown spectroscopy, Spectrochim. Acta Part B 78 (2012) 62–66.
[34] D. Cremers, L. Radziemski, Detection of chlorine and fluorine in air by laser induced breakdown spectrometry, Anal. Chem. 55 (1983) 1252–1256.
[35] M. Tran, Q. Sun, B. Smith, J. Winefordner, Determination of F, Cl, and Br in solid organic compounds by laser-induced plasma spectroscopy, Appl. Spectrosc. 55 (2001) 739–744.
[36] C. Alvarez, J. Pisonero, N. Bordel, Quantification of fluorine mass-content in powdered ores using a laser-induced breakdown spectroscopy method based on the detection of minor elements and CaF molecular bands, Spectrochim. Acta Part B 100 (2014) 123–128.
[37] L.J. Fernández-Menéndez, C. Méndez-López, C. Alvarez-Llamas, C. González-Gago, J. Pisonero, N. Bordel, Spatio-temporal distribution of atomic and molecular excited species in Laser-Induced Breakdown Spectroscopy: Potential implications on the determination of halogens, Spectrochim. Acta Part B 168 (2020), 105848.
[38] C. Álvarez-Llamas, J. Pisonero, N. Bordel, A novel approach for quantitative LIBS fluorine analysis using CaF emission in calcium-free samples, J. Anal. At. Spectrom. 32 (2017) 162–166.
[39] Q. Li, W. Zhang, Z. Tang, et al., Determination of fluorine content in rocks using laser-induced breakdown spectroscopy assisted with radical synthesis, Talanta 234 (2021), 122712.
[40] *Guidelines for Drinking-Water Quality: Fourth Edition Incorporating the First Addendum*, World Health Organization, 2017.
[41] S. Ali, S. Thakur, A. Sarkar, S. Shekhar, Worldwide contamination of water by fluoride, Environ. Chem. Lett. 14 (2016) 291–315.
[42] X. Yu, N. Jiang, X. Miao, F. Li, J. Wang, R. Zong, S. Lu, Comparative studies on foam stability, oil-film interaction and fire extinguishing performance for fluorine-free and fluorinated foams, Process Saf. Environ. Prot. 133 (2020) 201–215.
[43] C. McDonough, J. Guelfo, C. Higgins, Measuring total PFASs in water: The tradeoff between selectivity and inclusivity, Curr. Opin. Environ. Sci. Health 7 (2018) 13–18.
[44] P. Mello, J. Barin, F. Duarte, C. Bizzi, L. Diehl, E. Muller, E. Flores, Analytical methods for the determination of halogens in bioanalytical sciences: A review, Anal. Bioanal. Chem. 405 (2013) 7615–7642.
[45] D. Rusak, T. Anthony, Z. Bell, Note: A novel technique for analysis of aqueous solutions by laser-induced breakdown spectroscopy, Rev. Sci. Instrum. 86 (2015), 116106.
[46] Z. Tang, Z. Hao, R. Zhou, Q. Li, K. Liu, W. Zhang, J. Yan, K. Wei, X. Li, Sensitive Analysis of Fluorine and Chlorine elements in Water Solution using Laser-induced Breakdown Spectroscopy assisted with Molecular Synthesis, Talanta 224 (2021), 121784.
[47] C. Méndez-López, L.J. Fernández-Menéndez, C. González-Gago, J. Pisonero, N. Bordel, Nebulization assisted molecular LIBS for sensitive and fast fluorine determination in aqueous solutions, J. Anal. At. Spectrom. 38 (2023) 80–89.
[48] A. Ashori, Nonwood fibers - A potential source of raw material in papermaking, Polym. Plast. Technol. Eng. 45 (10) (2006) 1133–1136.
[49] M. Hubbe, R. Gil, Fillers for papermaking: a review of their properties, usage practices, and their mechanistic role, BioResources 11 (1) (2016) 2886–2963.
[50] C. Méndez-López, R. Álvarez-García, C. Alvarez-Llamas, L.J. Fernández-Menéndez, C. González-Gago, J. Pisonero, N. Bordel, Laser induced plasmas at different nebulization conditions: Spatio-temporal distribution of emission signals and excitation temperatures, Spectrochim. Acta Part B 170 (2020), 105906.
[51] L.J. Fernández-Menéndez, C. Méndez-López, C. González-Gago, et al., A critical evaluation of the chlorine quantification method based on molecular emission detection in LIBS, Spectrochim. Acta Part B 190 (2022), 106390.
[52] G. Long, J. Winefordner, Limit of Detection: a closer look at the IUPAC definition, Anal. Chem. 55 (7) (1983) 712A–724A.
[53] R. Russo, X. Mao, J. Yoo, J. Gonzalez, Laser ablation, in: J. Singh, S. Thakur (Eds.), Laser-Induced Breakdown Spectroscopy, second ed., Elsevier, Amsterdam, 2007, pp. 41–70.